Lymphatic endothelial cell calcium pulses are sensitive to spatial gradients in wall shear stress

Vinay N. Surya[a,†], Eleftheria Michalaki[a,†], Gerald G. Fuller[a], and Alexander R. Dunn[a,b,*]
[a]Department of Chemical Engineering, Stanford University, Stanford, CA 94305; [b]Stanford Cardiovascular Institute, Stanford University School of Medicine, Stanford, CA 94305

ABSTRACT **Cytosolic calcium (Ca^{2+}) is a ubiquitous second messenger that influences numerous aspects of cellular function. In many cell types, cytosolic Ca^{2+} concentrations are characterized by periodic pulses, whose dynamics can influence downstream signal transduction. Here, we examine the general question of how cells use Ca^{2+} pulses to encode input stimuli in the context of the response of lymphatic endothelial cells (LECs) to fluid flow. Previous work shows that fluid flow regulates Ca^{2+} dynamics in LECs and that Ca^{2+}-dependent signaling plays a key role in regulating lymphatic valve formation during embryonic development. However, how fluid flow might influence the Ca^{2+} pulse dynamics of individual LECs has remained, to our knowledge, little explored. We used live-cell imaging to characterize Ca^{2+} pulse dynamics in LECs exposed to fluid flow in an in vitro flow device that generates spatial gradients in wall shear stress (WSS), such as are found at sites of valve formation. We found that the frequency of Ca^{2+} pulses was sensitive to the magnitude of WSS, while the duration of individual Ca^{2+} pulses increased in the presence of spatial gradients in WSS. These observations provide an example of how cells can separately modulate Ca^{2+} pulse frequency and duration to encode distinct forms of information, a phenomenon that could extend to other cell types.**

Monitoring Editor
Alex Mogilner
New York University

Received: Oct 9, 2018
Revised: Feb 11, 2019
Accepted: Feb 19, 2019

INTRODUCTION

Calcium (Ca^{2+}) is a universal secondary messenger that exerts profound effects on cell proliferation, contractility, migration, and transcriptional regulation (Clapham, 2007). In mammalian cells, cytoplasmic Ca^{2+} concentrations are kept low (100 nM) relative to the extracellular environment. In many cell types, Ca^{2+} release into the cytoplasm is transient, as pumps in the endoplasmic reticulum and plasma membrane continually remove Ca^{2+} from the cytoplasm (Clapham, 2007; Smedler and Uhlén, 2014). As a result, Ca^{2+} signaling is driven not only by changes in average cytosolic concentrations, but also by the frequency of individual Ca^{2+} pulses (Dolmetsch, Xu, and Lewis, 1998; Smedler and Uhlén, 2014). The rich temporal dynamics that characterizes Ca^{2+} signaling can in principle provide the cell with the opportunity to encode multiple forms of information in, for example, Ca^{2+} pulse frequency and duration. Whether this in fact occurs is, to our knowledge, little explored.

Fluid flow is thought to play a central role in patterning the developing blood and lymphatic vasculatures (Dixon *et al.*, 2006; Sabine *et al.*, 2012, 2015; Planas-Paz and Lammert, 2013; Baeyens *et al.*, 2015; Jafarnejad *et al.*, 2015; Kornuta *et al.*, 2015; Sweet *et al.*, 2015; Cha *et al.*, 2016; Fatima *et al.*, 2016). Lymphatic endothelial cells (LECs) line lymphatic vessels and experience a wide range of flow-induced wall shear stresses (WSSs) depending on the local vessel geometry. Previous work indicates that WSS may regulate both the growth of lymphatic vessels (lymphangiogenesis) and the development of lymphatic valves (Dixon *et al.*, 2006; Sabine *et al.*, 2012, 2015; Planas-Paz and Lammert, 2013; Baeyens *et al.*, 2015;

This article was published online ahead of print in MBoC in Press (http://www.molbiolcell.org/cgi/doi/10.1091/mbc.E18-10-0618) on February 27, 2019.

†These authors contributed equally to this work.

The authors declare no actual or perceived conflicts of interest.

Author contributions: V.N.S. and E.M. conducted the research; V.N.S. and E.M. analyzed the data; all of the authors performed manuscript and figure preparation; G.G.F and A.R.D. supervised and supported the research.

*Address correspondence to: Alexander R. Dunn (alex.dunn@stanford.edu).

Abbreviations used: Ca^{2+}, calcium; CRAC, calcium release activated channel; DC, duty cycle; FWHM, full width half maximum; IFC, impinging flow chamber; IP3, inositol 1,4,5-trisphosphate; IP3R1, inositol 1,4,5-trisphosphate receptor type1; LECs, lymphatic endothelial cells; NFATc1, Nuclear Factor of Activated T Cells cytoplasmic 1; NP, nonperiodic; P, periodic; WSS, wall shear stress; WSSG, wall shear stress gradient.

Jafarnejad *et al.*, 2015; Kornuta *et al.*, 2015; Sweet *et al.*, 2015; Cha *et al.*, 2016; Fatima *et al.*, 2016; Choi *et al.*, 2017a,b). Interestingly both lymphatic and venous valves form preferentially near vessel constrictions and junctions, areas that feature large spatial variations in WSS, here termed WSS gradients (WSSGs) (Kampmeier and La Fleur Birch, 1927; Bazigou *et al.*, 2009; Sabine *et al.*, 2012; Planas-Paz and Lammert, 2013). However, how and whether WSSGs may act to regulate the timing and location of valve formation remains poorly understood.

Ca^{2+}-dependent signaling provides a potential link between the physical stimulus provided by fluid flow and the regulation of lymphatic development (Sabine *et al.*, 2012; Choi *et al.*, 2017a,b). The Ca^{2+} release–activated channel (CRAC) ORAI1 is required for lymphangiogenesis in mouse embryos (Choi *et al.* 2017b), and inhibition of ORAI1 with SKF-96365 in LECs in vitro blocks activation of Klf2, a transcription factor that is both activated in response to WSS and required for cellular reorientation with WSS (Choi *et al.* 2017a). The activity of ORAI1 is subject to Ca^{2+}-dependent feedback that is mediated in part by STIM1, a protein that senses Ca^{2+} levels in the endoplasmic reticulum (Soboloff *et al.*, 2006; Choi *et al.* 2017a; Cai *et al.*, 2018). Previous experiments indicate that WSS, and temporally varying WSS in particular, also leads to the activation of the Ca^{2+}-dependent phosphatase calcineurin (Sabine *et al.*, 2012). Calcineurin dephosphorylates the transcription factor Nuclear Factor of Activated T Cells cytoplasmic 1 (NFATc1), allowing it to accumulate in the nucleus (Clapham, 2007; Sabine *et al.*, 2012), where it participates in the initiation of valvulogenesis (Dixon *et al.*, 2006; Kulkarni *et al.*, 2009; Vittet, 2014; Kornuta *et al.*, 2015). NFAT-dependent transcriptional regulation can in turn potentially influence Ca^{2+} signaling: in hippocampal cells, Ca^{2+}-mediated activation of NFATc4 triggers the transcription of inositol 1,4,5-trisphosphate (IP3) receptor type1 (IP3R1), further elevating cytoplasmic Ca^{2+} (Crabtree, 2001). Such feedback loops can in principle be rapid on the time scale of development: both NFAT and NF-κB, a transcription factor thah like NFAT is known to be sensitive to Ca^{2+} cytoplasmic levels (Dolmetsch *et al.*, 1997; Smedler and Uhlén, 2014), relocalize to the nucleus in minutes in response to WSS (Yissachar, Sharar Fischler, *et al.*, 2013; Zhao *et al.*, 2018).

Although previous studies have examined Ca^{2+} signaling in LECs in response to spatially uniform WSS, little is known about how gradients in WSS may specifically regulate Ca^{2+} signaling. Further, to our knowledge, no previous study has characterized the dynamics of Ca^{2+} signaling in LECs at the individual cell level. Previously, we developed an impinging flow chamber (IFC) that imparts controlled WSSGs to adherent cells grown in a standard six-well tissue culture plate (Ostrowski *et al.*, 2014, 2015; Nakayama *et al.*, 2016; Surya *et al.*, 2016; Chang *et al.*, 2017). In this study, we used this device to determine how Ca^{2+} pulse dynamics in individual LECs respond to both the WSS magnitude and gradients in WSS. We found that both aspects of flow regulate Ca^{2+} pulse dynamics, and that WSSGs in particular increase Ca^{2+} pulse duration relative to uniform WSS. These and other observations indicate that both WSS magnitude and WSSGs can act as physical cues to regulate Ca^{2+} dynamics in LECs, suggesting that WSSGs provide a spatial cue that can potentially act to confine valvulogenesis to vessel constrictions and junctions.

RESULTS

Examination of Ca^{2+} pulse dynamics in human lymphatic microvascular endothelial cells subjected to a WSSG

In this study, we sought to investigate how WSS and WSSGs might modulate Ca^{2+} dynamics in LECs. To do so, we subjected human lymphatic microvascular endothelial cells (HLMVECs) to impinging flow, which generates a spatial WSSG that approximates the WSSGs found at a lymphatic vessel branch (Figure 1, A–C). LECs in vivo are likely exposed to 0–10 dyn/cm^2 (Dixon *et al.*, 2006). To fully characterize the response of these cells to WSS and WSSGs, we employed WSSs ranging from 0 to 72 dynes/cm^2. We reasoned that characterizing the response of cells to as wide a range in WSSs as possible would be valuable in understanding their response to fluid flow: an analogy would be treating cells with a wide range of concentrations of a soluble signaling factor in order to understand how it influenced intracellular signal transduction.

In other systems, pulse frequency often reflects the strength of a Ca^{2+}-activating stimulus; that is, increasing the external stimulus results in an increase in the Ca^{2+} pulse count (Smedler and Uhlén, 2014). In contrast, the pulse duration, here determined as the Ca^{2+} pulse full width at half maximum (FWHM), can reflect the signaling pathway(s) present in the cell that indirectly regulate Ca^{2+} influx and efflux (Smedler and Uhlén, 2014). The pulse duty cycle (DC), defined as the fraction of the time that cytosolic Ca^{2+} is above its baseline concentration, provides an alternate measure of the Ca^{2+} activation, with increasing DC values indicative of a stronger activation of Ca^{2+}-dependent signal transduction. Here, we used live-cell recordings to quantify Ca^{2+} pulse count, peak-to-peak period, and pulse full width at half maximum (pulse duration; FWHM) for individual cells (Figure 1, D and E; Supplemental Movies S1–S4). These data were binned by position with reference to the center of the jet orifice ($r = 0$). We also examined whether exposure to impinging flow triggered the nuclear localization of NFATc1, an event that occurs in response to Ca^{2+}-dependent signaling (Kulkarni *et al.*, 2009; Norrmén *et al.*, 2009; Sabine *et al.*, 2012; Smedler and Uhlén, 2014). As expected, we observed that nuclear NFATc1 was higher in HLMVECs exposed to impinging flow than in cells under no flow, indicative of downstream signaling in response to flow-activated Ca^{2+} pulses (Supplemental Figure S1).

We found that Ca^{2+} pulse dynamics was heterogeneous: some cells pulsed repeatedly, while others either did not pulse or pulsed once in the 30-min observation window. For cells that pulsed, the first pulse often corresponded roughly to the onset of flow at the beginning of the experiment; this initial pulse was shorter for cells that went on to pulse multiple times (termed P or periodic cells) than for cells that only pulsed once in the 30-min observation window (termed NP or nonperiodic; see Supplemental Figure S2). For P cells, subsequent pulses were longer in duration than that initial pulse, but only in the presence of a WSSG (Figure 2). This trend held for the subset of P cells that pulsed three or more times, suggesting that the initial pulse was indeed distinct from subsequent ones, though only for cells exposed to a WSSG (Supplemental Figure S3). In contrast, there were no significant differences in the duration of initial vs. subsequent Ca^{2+} pulses in the absence of flow. Together, these findings suggest that Ca^{2+} dynamics are both WSS- and WSSG-sensitive.

Ca^{2+} pulse count scales with local WSS

Ca^{2+} pulse frequency is often used as a reporter for the strength of upstream signaling activators, with increasing pulse frequency being indicative of a stronger stimulus (Smedler and Uhlén, 2014). We therefore sought to determine the role of WSS and WSSGs in modulating Ca^{2+} pulse frequency. Of the models tested, we found that a hierarchical gamma (Γ) Poisson model provided the best fit to the cumulative distribution of the number of pulses produced by the total population of cells in a 30-min time window (Figure 3). This model functions analogously to a Poisson distribution, but with an

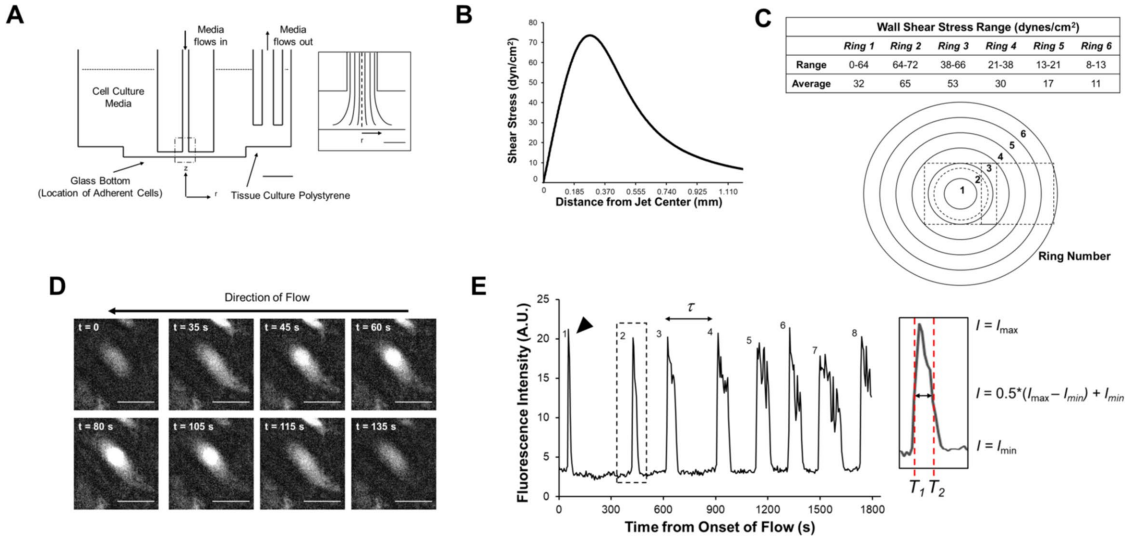

FIGURE 1: Measuring Ca^{2+} pulse dynamics using the IFC. (A) A cross section showing to scale the location of the jet orifice, which is submerged in medium inside each well. Scale bar, 5 mm. Inset: The dashed region of impinging flow in A. The shear stress profile is axisymmetric about $r = 0$. Scale bar, 500 µm. Adapted from Ostrowski *et al.* (2015). (B) WSS is plotted as a function of distance from the jet center at a flow rate of 4.5 ml/min. (C) Cells are binned by their position into one of six concentric 185-µm rings. The table summarizes the range and average WSS values for each ring. On the schematic, the dashed circle represents the location of the maximum WSS (72 dyn/cm^2) and the dashed squares represent the regions of image acquisition. (D) Fluorescence micrographs of a Ca^{2+} pulse for a representative HLMVEC (black triangle, E). In this example, a pulse begins soon after the onset of impinging flow ($t = 0$ s) and rises to a peak at $t = 80$ s. (E) Fluorescence intensity versus time for the cell shown in D, with the black triangle indicating the first observed pulse. The pulse count (i.e., how many pulses occur within the 30-min experimental time) and peak-to-peak period (τ, time between successive peaks) were determined for individual cells. The pulse duration was measured by calculating the full width at half maximum (FWHM) by measuring the difference in times T_1 and T_2 at half-maximum intensity.

average time between pulses that varies across individual cells according to a Γ distribution. Thus, this distribution can be used to characterize underlying heterogeneity that would be absent in a standard Poisson distribution.

Cells exposed to WSSGs in the impinging flow cell had appreciably higher average pulse counts than cells observed under no flow, with an average pulse count λ that scaled roughly with the local WSS (Figure 3). In particular, the fraction of P cells increased with increasing WSS to a maximum of ~0.6 (Table 1). These findings are in agreement with studies demonstrating that WSS is sufficient to trigger cytoplasmic Ca^{2+} release, including in HLMVECs (Shen *et al.*, 1992; Okuda, Takahashi, *et al.*, 1999; Jafarnejad *et al.*, 2015), but expand on previous work by revealing an underlying population heterogeneity. We also compared the pulse count distributions arising from cells in Ring 3 of the IFC with that arising from cells experiencing an equivalent, spatially uniform WSS in a parallel-plate flow chamber. Cells exposed to spatially uniform WSS of 50 dyn/cm^2 exhibited a slightly hgher pulse count ($\lambda = 3.1$ vs. 2.5, $p < 0.05$). However, the overall similarity of the pulse counts observed for these two conditions lends support to the argument that pulse count scales primarily with local WSS.

The variability in timing between pulses is parameterized by the shape parameter α, with a larger α indicating a closer approximation to a standard Poisson distribution. By this metric, the time intervals between pulses were most irregular under no flow ($\alpha = 0.4$), and most regular for cells near the center of the impinging flow ($\alpha = 4.0$), where the elongational stresses (i.e., stretching forces due to fluid flow) were largest. This observation suggests that gradients in WSS, such as are found at sites of valve formation, may serve to regularize the time intervals between Ca^{2+} pulses.

We next sought to determine whether differences in pulse count were spatially correlated among neighboring LECs. To do so, we used the *k*-means clustering algorithm to identify clusters of cells for every condition presented on Figure 3. We then determined the fraction of P cells for each cluster (Supplemental Figure S4). To determine whether P cells indeed clustered, we then randomly reassigned the measured cell-by-cell pulse counts and repeated the clustering algorithm. The resulting fractions of P cells per cluster were statistically indistinguishable from those observed experimentally (Supplemental Figure S5). Thus, while we do not rule out some form of local coordination among cells, the data are most consistent with the idea that pulse counts are regulated on an individual cell level rather than on a cluster level.

Exposure to WSSGs results in increased Ca^{2+} pulse duration

We next examined the pulse duration (FWHM) for both the initial pulse and the subsequent pulses in P cells (pulse count > 1). To do so, we fitted each distribution of pulse durations to a Weibull distribution (Figure 2), which is commonly used to model time-to-termination distributions. The Weibull distribution consists of a stretched exponential distribution with shape (κ) and scale (β) parameters such that the probability distribution *f* for the duration *T* of a pulse is

$$f(T;\beta,\kappa) = \frac{\kappa}{\beta}\left(\frac{T}{\beta}\right)^{\kappa-1} e^{-(T/\beta)^{\kappa}} \text{ when } T \geq 0.$$

The Weibull distribution reduces to an exponential distribution when the probability of a pulse terminating is constant in time following its initiation ($\kappa = 1$). We saw that κ changed from ≥1 for the initial pulse to <1 for the subsequent pulses in the presence of a

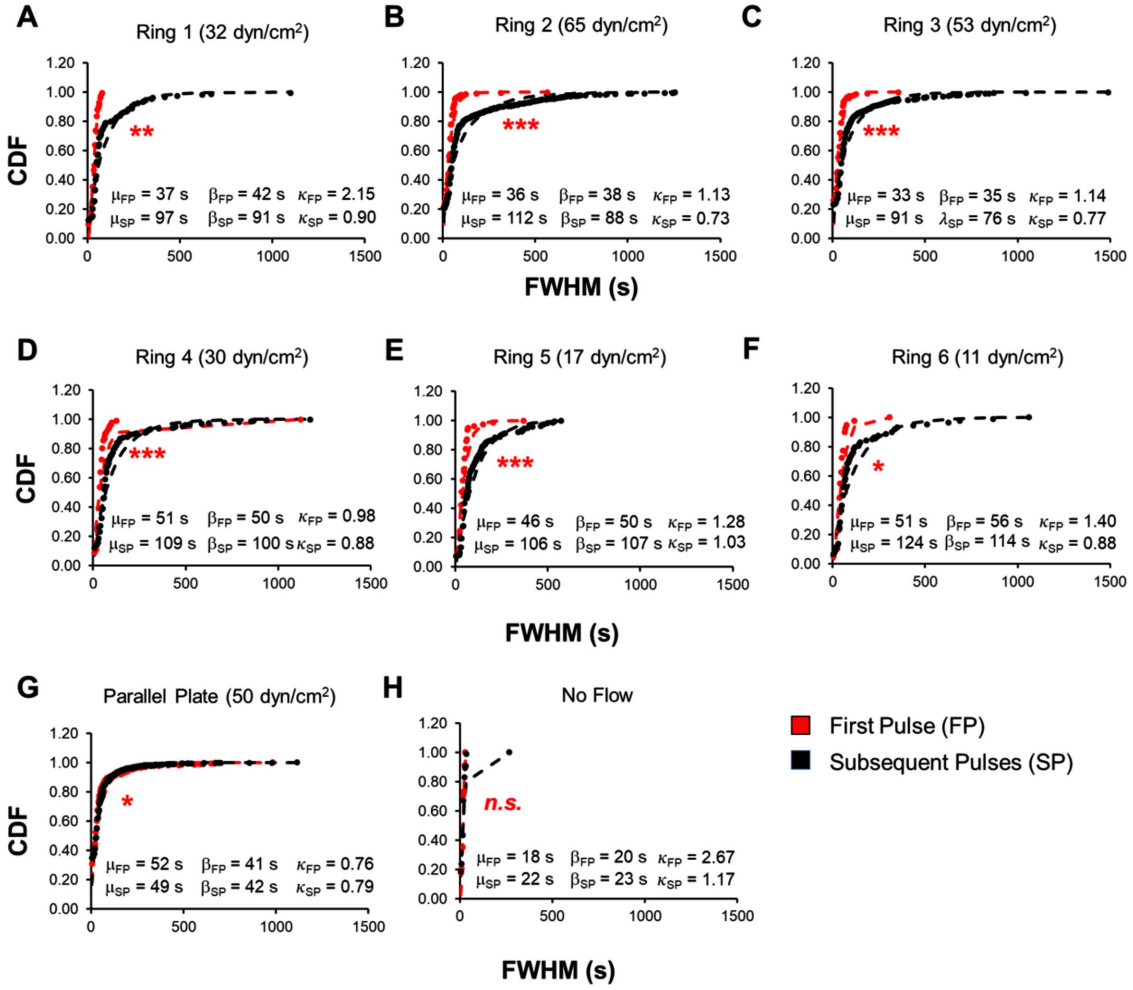

FIGURE 2: HLMVEC Ca^{2+} pulse durations are sensitive to WSS magnitude and WSSGs in cells that pulse repeatedly. Plots represent the cumulative distribution functions (CDFs) for individual pulse durations (measured as FWHM) for P cells. The initial pulse (first pulse, FP) is shown in red, while all subsequent pulses (second, third, etc., SP) are shown in black. Dotted lines are fits to the Weibull distribution (see text). Pulse duration distributions are portrayed for Rings 1–6 (A–F), spatially uniform WSS (parallel plate chamber, G), and no flow (H). The scale (β) and shape (κ) parameters for fits to the Weibull distribution and the average pulse durations (FWHM; μ) are presented at the bottom of each graph. Experiments were performed in triplicate. Asterisks indicate statistically significant differences in CDFs as determined using the Kolmogorov–Smirnov test (*n.s.*, not significant; *, $p < 0.05$; **, $p < 10^{-4}$; ***, $p < 10^{-7}$).

WSSG with the exception of Ring 5, while it remained less than one under uniform flow and greater than one in the absence of flow. These differences are consistent with an increase in pulse duration with pulse number that occur in the presence of a WSSG but not spatially uniform WSS or the absence of flow (Supplemental Figure S3). Thus, WSSGs drove a gradual increase of Ca^{2+} pulse duration, whereas spatially uniform WSS did not.

WSSGs increase DC but not pulse frequency in P cells

We also examined how WSS and WSSGs affected the DC, which we define here exclusively for P cells. We first sought to determine the time between consecutive pulses (peak-to-peak period), which would influence the DC. We observed that the time between consecutive pulses was shorter under flow conditions as compared with that in the absence of flow (Figure 4A). Interestingly, the peak-to-peak period was relatively constant in cells subjected to flow regardless of whether they experienced a gradient in WSS. To investigate this further, we examined the periodicity of repeatedly pulsing cells and observed little to no difference in the time between consecutive pulses (Supplemental Figure S6). In contrast, pulse durations for P cells exposed to WSSG, regardless of the absolute WSS magnitude, were twofold higher than those of P cells in the presence of a spatially uniform WSS, and four- to fivefold higher than those of P cells under no flow (Figure 2). In consequence, DCs measured for HLMVECs exposed to WSSGs were almost twofold higher than those measured for cells exposed to spatially uniform, 50 dyn/cm^2 WSS, and fourfold higher as compared with cells under no flow (Figure 4B). Thus, the presence of a WSSG increased the strength of Ca^{2+} activation relative to a spatially uniform WSS, regardless of the magnitude of WSS.

DC is influenced by both CRAC channel and calcineurin activity

Previous studies identified roles for the CRAC channel ORAI1 and the Ca^{2+}-dependent phosphatase calcineurin in lymphatic development (Kulkarni *et al.*, 2009; Sabine *et al.*, 2012; Choi *et al.* 2017a,b).

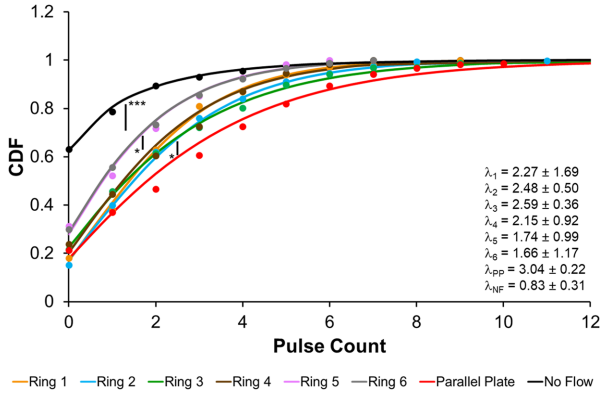

FIGURE 3: Ca^{2+} pulse count is WSS- and WSSG-dependent. CDF plots of Ca^{2+} pulse counts for HLMVECs exposed to either impinging flow (Rings 1–6), spatially uniform flow (parallel plate chamber; PP), or no flow (NF) for 30 min. HLMVECs are binned by location relative to the jet center (Figure 1, B and C). Dots indicate the measured CDF, while the solid line is a fit to a Γ-Poisson distribution. The parameter λ is the fit value for the average pulse count for the distribution and is presented in the lower right-hand corner. Experiments were performed in triplicate. Asterisks indicate statistically significant differences in CDFs as determined using the Kolmogorov–Smirnov test (*n.s.*, not significant; *, $p < 0.05$; **, $p < 10^{-4}$; ***, $p < 10^{-7}$).

We therefore examined whether either or both proteins might help to set Ca^{2+} pulse dynamics in response to WSS and/or WSSGs. We observed a significant decrease in the DC when HLMVECs were treated with either 10 μM SKF96365 (ORAI1 inhibitor, IC_{50} = 10 μM) or 5 μM cyclosporin A (calcineurin inhibitor; CsA, IC_{50} = 5 nM) for 1 h prior to the onset of impinging flow (Figure 5 and Supplemental Figures S7–S11). This decrease in DC appeared to be due in part to a decrease in pulse frequency for both inhibitors (Supplemental Figure S9). Also, inhibition of ORAI1 decreased pulse duration for P cells across Rings 2–5, while calcineurin inhibition decreased pulse duration in Rings 5 and 6 (Supplemental Figures S10 and S11). A plausible interpretation is that both ORAI1 and calcineurin are required for normal Ca^{2+} pulse dynamics, consistent with possible feedback mediated by both proteins. However, we cannot exclude the possibility that either or both inhibitors acted through alternative pathways in our experiments.

DISCUSSION

Previous work has established that Ca^{2+}-dependent activation of NFATc1 is essential for the formation of lymphatic valves (Kulkarni *et al.*, 2009; Norrmén *et al.*, 2009; Sabine *et al.*, 2012; Planas-Paz and Lammert, 2013; Vittet, 2014). However, how exactly the activation of NFATc1 is confined to regions of valvulogenesis is unclear, as fluid flow is present throughout the lymphatic system. We found that both the fraction of P cells and the number of pulses scaled roughly with WSS, providing a mechanism by which LECs can encode the local WSS magnitude (Figure 3 and Table 1). This finding is consistent with and extends a previous report that the average cytoplasmic Ca^{2+} concentrations in HLMVECs increase with increasing WSS (Jafarnejad *et al.*, 2015). Importantly, we also found that for P cells exposed to a WSSG, the DC was ~0.3 regardless of the local WSS, and about twice that observed for LECs exposed to spatially uniform WSS (Figure 4B). A Ca^{2+} DC of 0.3 was previously shown to lead to maximal NFATc1 activation in Jurkat T-cells (Dolmetsch *et al.*, 1997; Dolmetsch, Xu, and Lewis, 1998; Tsien *et al.*, 1998; Smedler and Uhlén, 2014). We suggest that the marked increase in DC in the presence of a WSSG may provide a robust means of patterning valve formation by confining NFATc1 activation to regions that feature large gradients in WSS such as vessel constrictions and branches, precisely the regions where valve formation is favored.

Although Ca^{2+}-mediated signaling in ECs in response to fluid flow has been examined (Ando *et al.*, 1988; Schwarz *et al.*, 1992; Shen *et al.*, 1992; Helmlinger *et al.*, 1996; Okuda, Takahashi, *et al.*, 1999; Jafarnejad *et al.*, 2015), to our knowledge a single-cell analysis of pulse kinetics such as we report here has not been performed previously. This analysis allowed us to distinguish between the responses of LECs to different input stimuli (spatially uniform WSS vs. WSSGs) and to infer that the Ca^{2+} signaling in response to the onset of flow differed from the response to sustained flow. We anticipate that the analysis approaches developed here may be useful for characterizing Ca^{2+} signaling in a variety of experimental systems.

Whether the cells that pulse repeatedly (P), once, or zero times reflect distinct subpopulations present in the primary cells used in our experiments is unclear. The fact that the fraction of cells that pulsed at least once varied with WSS magnitude argues that cells can convert between pulsing and nonpulsing states. On the other hand, we cannot definitively rule out that the ~20% of cells that did not pulse in the observed time window even under the largest WSS may belong to a subpopulation of cells in which flow does not activate Ca^{2+} signaling.

The identity of the flow sensors that control the Ca^{2+} dynamics we describe is unclear. Endothelial cells have been proposed to sense flow via the activation of multiple transmembrane receptors and complexes, including the VEGFR2/PECAM-1/VE-Cadherin/VEGFR3 complex, G-protein coupled receptors (GPR68, Bradykinin B2),

	Average WSS (dyn/cm²)	μ	Fraction of P cells	α (shape)	β (interval)	λ = α/β
Ring 1	32	2.25	0.62	4.03	1.78	2.27 ± 1.69
Ring 2	65	2.45	0.60	2.80	1.13	2.48 ± 0.50
Ring 3	53	2.48	0.54	1.58	0.61	2.59 ± 0.36
Ring 4	30	2.19	0.56	2.63	1.22	2.15 ± 0.92
Ring 5	17	1.69	0.48	2.41	1.38	1.74 ± 0.99
Ring 6	11	1.68	0.45	2.20	1.32	1.66 ± 1.17
Parallel plate	50	3.07	0.63	1.64	0.54	3.04 ± 0.22
No flow	n/a	0.84	0.22	0.43	0.51	0.83 ± 0.31

The average WSS, experimental mean μ, fraction of P cells, and parameters from a fit to the hierarchical Γ-Poisson are listed from left to right. λ is the mean predicted from the fit to the Γ-Poisson distribution (modeled by the shape parameter, α, and the interval parameter, β).

TABLE 1: Modeling parameters for the Ca^{2+} pulse count measurements in Figure 3.

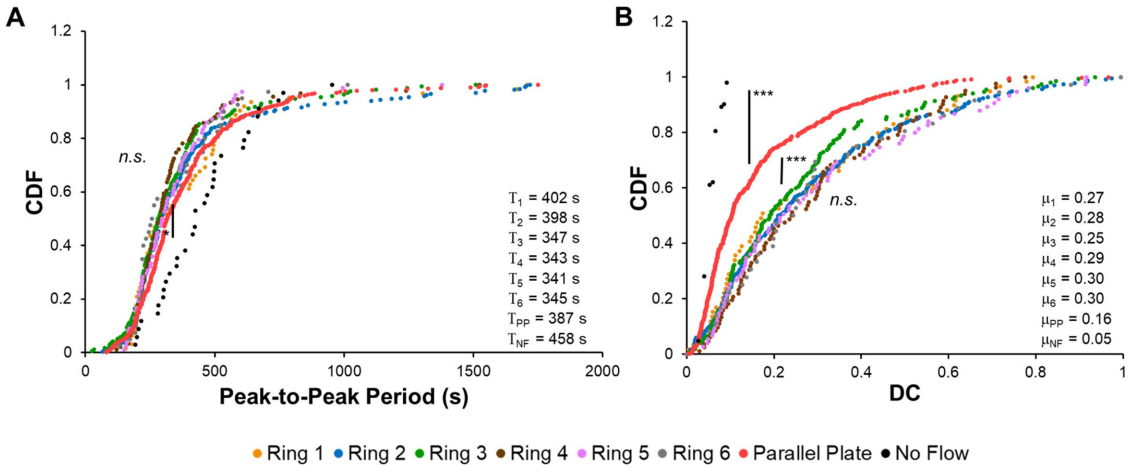

FIGURE 4: WSSG modulates the Ca^{2+} pulse duty cycle but not the pulse period. CDF plots for the (A) average peak-to-peak period per cell and (B) duty cycle (DC) per cell for Ca^{2+} pulses in HLMVECs exposed to impinging flow, parallel plate flow, or no flow. The average period and DC for each distribution are presented in the lower right-hand corner of each graph. Experiments were performed in triplicate. Asterisks indicate statistically significant differences in CDFs as determined using the Kolmogorov–Smirnov test (*n.s.*, not significant; *, $p < 0.05$; **, $p < 10^{-4}$; ***, $p < 10^{-7}$).

primary cilia, and stretch-activated ion channels (Tzima *et al.*, 2005; Chachisvilis *et al.*, 2006; Nauli *et al.*, 2008; Li, Hou, *et al.*, 2014; Ranade, Qiu, *et al.*, 2014; Baeyens *et al.*, 2015; Coon *et al.*, 2015; Fotiou, Martin-Almedina, *et al.*, 2015; Ellefsen, Chang, Nourse, *et al.*, 2018; Xu *et al.*, 2018). Several of these, including Bradykinin B_2, Piezo1 and VEGFR2 and -3 can potentially trigger downstream Ca^{2+} signaling through canonical signaling pathways (Tzima *et al.*, 2005; Clapham, 2007; Baeyens *et al.*, 2015). Which of these (or other) pathways are modulated specifically by WSSGs remains unknown, and an interesting topic for future investigations. Our observations suggest that calcineurin, whose activation lies downstream of cytosolic Ca^{2+}, may in turn regulate Ca^{2+} pulse dynamics, suggestive of a positive feedback loop. Whether this indeed occurs, and whether it helps to drive LEC commitment to the valvular phenotype, is likewise a target for future work.

MATERIALS AND METHODS

Cell culture

HLMVECs (CC-2810) were purchased from Lonza Corporation (Walkersville, MD) and cultured in EGM-2 basal medium (Lonza CC-3156) with supplements and growth factors (Lonza CC-4147) containing 5% FBS (fetal bovine serum), hEGF, VEGF, hFGF-B, R3-IGF-1, hydrocortisone, and ascorbic acid. Penicillin (50 U/ml) and streptomycin (50 µg/ml; Life Technologies, Carlsbad, CA) were added to the medium. Cells used for experiments were between passages 6 and 8. Three to five days before the experiment, depending on the desired initial confluency, cells were plated onto a six-well cell culture dish with a #1.5 glass coverslip bottom (Cellvis, Sunnyvale, CA). These dishes were precoated with 0.2% gelatin (Sigma-Aldrich, Saint Louis, MO) for 1 h. Cells were plated at 0.5–1.5 × 10^5 cells per dish and incubated at 37°C and 5% CO_2. We performed uniform WSS experiments using parallel plate flow chambers. The channels were also precoated with 0.2% gelatin. Cells were plated at 7.5 × 10^4 cells per well on each chamber and incubated at 37°C and 5% CO_2.

For flow experiments, Leibovitz's L-15 medium (Life Technologies) was used instead of EGM-2 to allow imaging independent of CO_2. The L-15 medium included 5% FBS, the endothelial growth factor kit from Lonza (CC-4147), 50 U/ml penicillin, and 50 µg/ml streptomycin (Life Technologies). LEC experiments were performed with cells at surface coverages (fractions of the coverslip covered by cells) of greater than 95% and confluency (fraction of maximum cell density) of 80% to ensure sufficient contact with neighboring cells.

Calcium dye treatment

Prior to the experiment, the EGM-2 media used to culture the HLMVECs were switched with the L-15 media (1.5 ml per well) described above. The plate containing the HLMVECs was then transferred to our custom-designed temperature-control chamber, used to keep the ambient temperature at 37°C during live-cell imaging. To perform live-cell imaging of Ca^{2+} dynamics, we used the Fluo-4 direct calcium assay kit (F10471; Thermo-Fisher Scientific, Waltham, MA). The kit contains three components: a Fluo4 Direct calcium assay reagent, a Fluo-4 Direct calcium assay buffer, and a proprietary water-soluble probenecid, which is added as described by Thermo-Fisher Scientific to prevent extrusion of the dye from cells. This custom formulation provides a stable and homogeneous fluorescence profile with low background fluorescence. A 250-mM stock solution probenecid was prepared by adding 1 ml of the supplied buffer to 77 mg of water-soluble probenecid. Resuspension and mixing through vortexing were performed until the reagent was completely dissolved. The dye formulation was made by adding 10 ml of the buffer to an entire bottle of the supplied dye and resuspending until dissolved; the resulting solution was dark red. Afterward, 200 µl of the prepared stock solution of probenecid was added to the prepared dye, and the resulting solution was vortexed thoroughly. The dye solution was then ready for use during flow experiments.

For Ca^{2+} imaging experiments, 500 µl of the prepared dye solution (optimized for HLMVEC flow experiments, 1:4 dilution in L-15) was incubated with the designated well of HLMVECs in the dark. Due to long–time scale cytotoxicity and the inevitable extrusion from the cells, the dye was added to each experimental well no more than 30 min before the beginning of imaging.

Fluid dynamics

Details of the fluid dynamics of the IFC have been reported previously (Ostrowski *et al.*, 2015; Surya *et al.*, 2016). Briefly, the IFC contains six submerged jet orifices that apply an impinging flow of cell culture media to a monolayer of adherent cells in standard glass-bottom six-well dishes. (Figure 1A). A nine-roller dampened peristaltic pump (Idex, Oak Harbor, WA) applied a flow of cell culture media

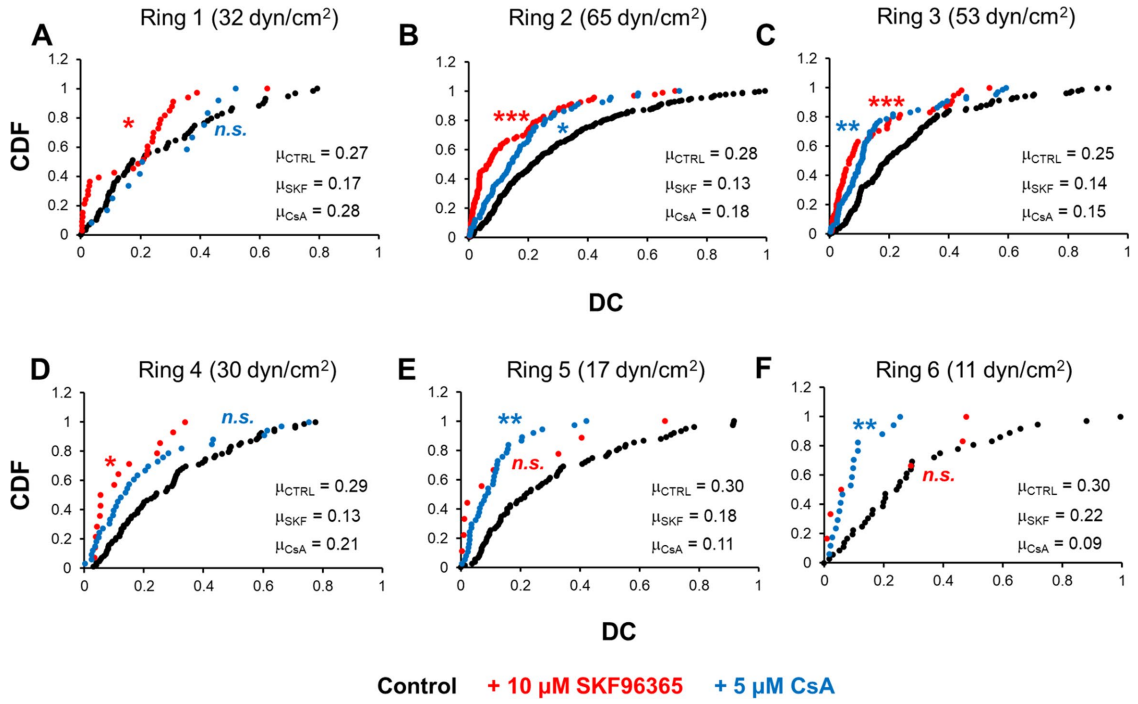

FIGURE 5: Treatment with ORAI1 and calcineurin inhibitors decreases Ca^{2+} DC. HLMVECs were treated with either 10 μM SKF96365 or 5 μM CsA or left untreated and exposed to impinging flow. CDF plots of the average DC per cell are presented for each condition. The average DC for each distribution is presented at the lower right-hand corner of each graph. Experiments were performed in duplicate. Asterisks indicate statistically significant differences in CDFs with respect to the untreated control as determined using the Kolmogorov–Smirnov test (*n.s.*, not significant; *, $p < 0.05$; **, $p < 10^{-4}$; ***, $p < 10^{-7}$).

at a flow rate of 4.5 ml/min. This flow rate provided a wide range of WSSs (0–72 dyn/cm^2) to the monolayer of HLMVECs and maximized the WSSG experienced across Rings 1–6 (Figure 1, B and C). In addition, we have previously reported that this range triggers flow-mediated collective upstream migration in HLMVECs on a 24-h timescale and that the HLMVEC migratory response to a 0–72 dyn/cm^2 range in WSS was qualitatively similar to their migratory response to a range of 0–10 dyn/cm^2 in WSS (Ostrowski *et al.*, 2014, 2015; Surya *et al.*, 2016).

Before the cells were exposed to impinging flow, the IFC was prepared by adding 10 ml of L-15 medium to each of the six chambers in the absence of cells followed the removal of bubbles. Media was circulated through the device tubing. Once the tubing lines were filled, the device was stopped, and the remaining air was removed using a syringe attached to a side port. All flow experiments were performed for 30 min. Cleaning of the device after the conclusion of an experiment was performed analogously to the device preparation above and performed as detailed previously (Surya *et al.*, 2016). All parallel plate experiments were performed with a uniform WSS of 50 dyn/cm^2 (comparable to the average WSS of Ring 3).

Fluorescence images were visualized using a Nikon Ti microscope (Nikon Corporation) with an Andor Neo Camera (Andor Technology, Belfast, UK), a Heliophor light engine providing excitation at 488 nm (89 North, Burlington, VT) and a 20× air objective (Nikon). A frame rate acquisition of once per 5 s was chosen based on prior in vitro studies demonstrating that the shortest observed Ca^{2+} pulses in ECs are ~15 s in duration (Jafarnejad *et al.*, 2015; Yokota *et al.*, 2015). Two regions were recorded per sample condition to visualize all six rings (Figure 1C): one region contains the IFC jet center (at $r = 0$) and the entirety of Rings 1 and 2 (Jet Center, "JC"; ~50 cells each ring) while the other was located in Rings 3 through 6 (Far Rings, "FR"; contains on average at least 25–30 cells per ring).

Inhibitor treatment

Our prior publications outline extensive inhibitor- and RNA interference–based studies using the IFC (Ostrowski *et al.*, 2015; Surya *et al.*, 2016). Each well of the six-well IFC is connected to a separate reservoir of cell culture medium, allowing six simultaneous, independent experiments. Generally, one JC and two FR measurements are performed per inhibitor experiment, along with the respective no-inhibitor control, subjected to identical flow conditions.

Stock concentrations of inhibitors were diluted in L-15 medium and added 1 h before the start of flow experiments. The inhibitor was also included in the recirculating medium to maintain its concentration throughout the experiment. SKF96365, a ORAI1 inhibitor, was purchased from Cayman Chemical (Ann Arbor, MI) (Item 10009312, CAS 130495-35-1) and a stock concentration was prepared in cell-culture grade dimethylsulfoxide (4–X; American Type Culture Collection, Manassas, VA), followed by dilution in L-15 to a final concentration of 10 μM. Cyclosporin A, a calcineurin inhibitor, was purchased from Sigma–Aldrich (Item 30024, CAS 59865-13-3) and a stock concentration was prepared in DMSO, followed by dilution in L-15 to a final concentration of 5 μM.

Immunofluorescence

At the end of the experiment, cells in the glass-bottom six-well dishes were fixed with 4% paraformaldehyde (43368, Alfa Aesar, Haverhill, MA) in PBS for 15 min, followed by two washes with PBS (2 min each), permeabilization for 10 min with 0.5% Triton X-100 (Sigma-Aldrich) and blocking for 1.5 h with 1% BSA in PBS. All these steps were performed at room temperature. Anti-human NFATc1

rabbit polyclonal antibody (1:250; ab25916, Burlingame, CA) and anti-human CD144 (1:500, VE-Cadherin) mouse antibody (555661, BD Pharmingen, San Jose, CA) were incubated overnight with the samples at 4°C. Secondary fluorescent antibodies anti-rabbit or mouse IgG Fab2 AlexaFluor Molecular Probes (4412S, 4410S, Cell Signaling Technology, Danvers, MA) were incubated with the samples for 1.5 h at room temperature in the dark (samples covered with aluminum foil). ActinRed 555 Ready Probes reagent (R37112, Thermo-Fisher Scientific) was used to stain actin and was incubated for 10 min at room temperature, followed by the addition of Hoechst (34580, Thermo-Fisher Scientific) to stain cell nuclei. Samples were visualized using the same Nikon Ti microscope, Andor Neo Camera, and 20× (air) objective as used for the calcium imaging experiments. Quantification of nuclear fluorescence intensity is presented in the Supplemental Information.

Analysis of calcium dynamics

Details of the analysis performed can be found in the Supplemental Information. Briefly, images were acquired in 16-bit format (2560 × 2160), binned, and downscaled to 8-bit format (640 × 540) before analysis using the Fiji (ImageJ) software. The available StackReg image stack registration macro was used to correct for minor stage drift. (Cells did not move appreciably over the course of the 30-min measurement.) A custom routine was created to track the total cellular fluorescence intensity per cell per frame, along with the cells' initial positions. These data were imported into MATLAB for analysis of pulse frequency, duration, and periodicity (Figure 1E). Cumulative distribution function plots and modeling of the distributions of experimental data were performed using MATLAB. We employed a Weibull fit for pulse duration measurements (Figure 2), while a Γ-Poisson fit was used to describe pulse count distributions (Figure 3). The shape and rate parameters α and β determine the Γ-Poisson fit to each pulse count distribution and are determined through a negative binomial distribution fit via MATLAB and conversion to the Γ-Poisson parameters.

ACKNOWLEDGMENTS

This work was supported in part by an American Heart Association Predoctoral Fellowship (16PRE27500024; V.N.S.), an Alexander S. Onassis Foundation Graduate Scholarship (E.M.), and an A.G. Leventis Foundation Graduate Scholarship (E.M.) and by the National Institutes of Health (R01HL128779).

REFERENCES

Boldface names denote co–first authors.

Ando J, Komatsuda T, Kamiya A (1988). Cytoplasmic calcium response to fluid shear stress in cultured vascular endothelial cells. In Vitro Cell Dev Biol 24, 871–877.

Baeyens N, Nicoli S, Coon BG, Ross TD, Van Den Dries K, Han J, Lauridsen HM, Mejean CO, Eichmann A, Thomas J-L, *et al*. (2015). Vascular remodeling is governed by a VEGFR3-dependent fluid shear stress set point. ELife 4, 1–35.

Bazigou E, Xie S, Chen C, Weston A, Miura N, Sorokin L, Adams R, Muro AF, Sheppard D, Makinen T (2009). Integrin-α9 is required for fibronectin matrix assembly during lymphatic valve morphogenesis. Dev Cell 17, 175–186.

Cai X, Nwokonko RM, Loktionova NA, Abdulqadir R, Baraniak JH, Wang Y, Trebak M, Zhou Y, Gill DL (2018). Pore properties of Orai1 calcium channel dimers and their activation by the STIM1 ER calcium sensor. J Biol Chem 293, 12962–12974.

Cha B, Geng X, Mahamud MR, Fu J, Mukherjee A, Kim Y, Jho E-H, Kim TH, Kahn ML, Xia L, *et al*. (2016). Mechanotransduction activates canonical Wnt/β-catenin signaling to promote lymphatic vascular patterning and the development of lymphatic and lymphovenous valves. Genes Deve 30, 1454–1469.

Chachisvilis M, Zhang YL, Frangos JA (2006). G protein-coupled receptors sense fluid shear stress in endothelial cells. Proc Natl Acad Sci USA 103, 15463–15468.

Chang AH, Raftrey BC, D'Amato G, Surya VN, Poduri A, Chen HI, Goldstone AB, Woo J, Fuller GG, Dunn AR, Red-Horse K (2017). DACH1 stimulates shear stress-guided endothelial cell migration and coronary artery growth through the CXCL12-CXCR4 signaling axis. Genes Dev 31,1308–1324.

Choi D, Park E, Jung E, Seong YJ, Hong M, Lee S, Burford J, Gyarmati G, Peti-Peterdi J, Srikanth S, *et al*. (2017a). ORAI1 activates proliferation of lymphatic endothelial cells in response to laminar flow through Krüppel-like Factors 2 and 4. Circ Res 120, 1426–1439.

Choi D, Park E, Jung E, Seong YJ, Yoo J, Lee E, Hong M, Lee S, Ishida H, Burford J, *et al*. (2017b). Laminar flow downregulates notch activity to promote lymphatic sprouting. J Clin Investig 127, 1225–1240.

Clapham DE (2007). Calcium signaling. Cell 131, 1047–1058.

Coon BG, Baeyens N, Han J, Budatha M, Ross TD, Fang JS, Yun S, Thomas J-L, Schwartz MA (2015). Intramembrane binding of VE-cadherin to VEGFR2 and VEGFR3 assembles the endothelial mechanosensory complex. J Cell Biol 208, 975–986.

Crabtree GR (2001). Calcium, calcineurin, and the control of transcription. J Biol Chem 276, 2313–2316.

Dixon JB, Greiner ST, Gashev AA, Cote GL, Moore JE, Zawieja DC (2006). Lymph flow, shear stress, and lymphocyte velocity in rat mesenteric prenodal lymphatics. Microcirculation 13, 597–610.

Dolmetsch RE, Lewis RS, Goodnow CC, Healy JI (1997). Differential activation of transcription factors induced by Ca^{2+} response amplitude and duration. Nature 386, 855–858.

Dolmetsch RE, Xu K, Lewis RS (1998). Calcium oscillations increase the efficiency and specificity of gene expression. Nature 392, 933–936.

Ellefsen K, Chang A, Nourse JL, Holt JR, Arulmoli J, Mekhdjian A, Flanagan LA, Dunn AR, Parker I, Pathak MM (2018). Piezo1 calcium flickers localize to hotspots of cellular traction forces. BioRxiv 294611.

Fatima A, Wang Y, Uchida Y, Norden P, Liu T, Culver A, Dietz WH, Culver F, Millay M, Mukouyama Y-S, Kume T (2016). Foxc1 and Foxc2 deletion causes abnormal lymphangiogenesis and correlates with ERK hyperactivation. J Clin Invest 126, 2437–2451.

Fotiou E, Martin-Almedina S, Simpson MA, Lin S, Gordon K, Brice G, Atton G, Jeffery I, Rees DC, Mignot C, *et al*. (2015). Novel mutations in PIEZO1 cause an autosomal recessive generalized lymphatic dysplasia with non-immune hydrops fetalis. Nat Commun 6, 8085.

Helmlinger G, Berk BC, Nerem RM (1996). Pulsatile and steady flow-induced calcium oscillations in single cultured endothelial cells. J Vasc Res 33, 360–369.

Jafarnejad M, Cromer WE, Kaunas RR, Zhang SL, **Zawieja DC, Moore JE** (2015). Measurement of shear stress-mediated intracellular calcium dynamics in human dermal lymphatic endothelial cells. Am J Physiol Heart Circ Physiol 308, H697–H706.

Kampmeier OF, La Fleur Birch C (1927). The origin and development of the venous valves, with particular reference to the saphenous district. Am J Anat 38, 451–499.

Kornuta JA, Nepiyushchikh Z, Gasheva OY, Mukherjee A, Zawieja DC, Dixon JB (2015). Effects of dynamic shear and transmural pressure on wall shear stress sensitivity in collecting lymphatic vessels. Am J Physiol Regul Integr Comp Physiol 309, 1122–1134.

Kulkarni RM, Greenberg JM, Akeson AL (2009). NFATc1 regulates lymphatic endothelial development. Mech Dev 126, 350–365.

Li J, Hou B, Tumova S, Muraki K, Bruns A, Ludlow MJ, Sedo A, Hyman AJ, McKeown L, Young RS, *et al*. (2014). Piezo1 integration of vascular architecture with physiological force. Nature 515, 279–282.

Nakayama KH, Surya VN, Gole M, Walker T, Yang W, Lai ES, Ostrowski M, Fuller GG, Dunn AR, Huang NF (2016). Nanoscale patterning of extracellular matrix alters endothelial function under shear stress. Nano Lett 16, 410–419.

Nauli SM, Kawanabe Y, Kaminski JJ, Pearce WJ, Ingber DE, Zhou J (2008). Endothelial cilia are fluid shear sensors that regulate calcium signaling and nitric oxide production through polycystin-1. Circulation 117, 1161–1171.

Norrmén C, Ivanov KI, Cheng J, Zangger N, Delorenzi M, Jaquet M, Miura N, Puolakkainen P, Horsley V, Hu J, *et al*. (2009). FOXC2 controls formation and maturation of lymphatic collecting vessels through cooperation with NFATc1. J Cell Biol 185, 439-4-457.

Okuda M, Takahashi M, Suero J, Murry CE, Traub O, Kawakatsu H, Berk BC (1999). Shear stress stimulation of $p130^{cas}$ tyrosine phosphorylation

requires calcium-dependent c-Src activation. J Biol Chem 274, 26803–26809.
Ostrowski MA, Huang EY, Surya VN, Poplawski C, Barakat JM, Lin GL, Fuller GG, Dunn AR (2015). Multiplexed fluid flow device to study cellular response to tunable shear stress gradients. Ann Biomed Eng 44, 1–12.
Ostrowski MA, Huang NF, Walker TW, Verwijlen T, Poplawski C, Khoo AS, Cooke JP, Fuller GG, Dunn AR (2014). Microvascular endothelial cells migrate upstream and align against the shear stress field created by impinging flow. Biophys J 106, 366–374.
Planas-Paz L, Lammert E (2013). Mechanical forces in lymphatic vascular development and disease. Cell Mol Life Sci 70, 4341–4354.
Ranade SS, Qiu Z, Woo S-H, Hur SS, Murthy SE, Cahalan SM, Xu J, Mathur J, Bandell M, Coste B, *et al*. (2014). Piezo1, a mechanically activated ion channel, is required for vascular development in mice. Proc Natl Acad Sci USA 111, 10347–10352.
Sabine A, Agalarov Y, Maby-El HH, Jaquet M, Hägerling R, Pollmann C, Bebber D, Pfenniger A, Miura N, Dormond O, *et al*. (2012). Mechanotransduction, PROX1, and FOXC2 cooperate to control Connexin37 and calcineurin during lymphatic-valve formation. Dev Cell 22, 430–45.
Sabine A, **Bovay E, Demir CS,** Kimura W, Jaquet M, Agalarov Y, Zangger N, Scallan JP, Graber W, Gulpinar E, *et al*. (2015). FOXC2 and fluid shear stress stabilize postnatal lymphatic vasculature. J Clin Invest 125, 3861–3877.
Schwarz G, Droogmans G, Nilius B (1992). Shear stress induced membrane currents and calcium transients in human vascular endothelial cells. Pflugers Arch 421, 394–396.
Shen J, Luscinskas FW, Connolly A, Forbes Dewey C, Gimbrone MA (1992). Fluid shear stress modulates cytosolic free calcium in vascular endothelial cells. Am J Physiol 262, C384–C390.
Smedler E, Uhlén P (2014). Frequency decoding of calcium oscillations. Biochim Biophys Acta 1840, 964–969.
Soboloff J, Spassova MA, Tang XD, Hewavitharana T, Xu W, Gill DL (2006). Orai1 and STIM reconstitute store-operated calcium channel function. J Biol Chem 281, 20661–20665.
Surya VN, Michalaki E, Huang EY, Fuller GG, Dunn AR (2016). Sphingosine 1-phosphate receptor 1 regulates the directional migration of lymphatic endothelial cells in response to fluid shear stress. J R Soc Interface 13, 20160823.
Sweet DT, Jiménez JM, Chang J, Hess PR, Mericko-Ishizuka P, Fu J, Xia L, Davies PF, Kahn ML (2015). Lymph flow regulates collecting lymphatic vessel maturation *in vivo*. J Clin Invest 125, 2995–3007.
Tsien RY, Li WH, Llopis J, Whitney M, Zlokarnik G (1998). Cell-permeant caged $InsP_3$ ester shows that Ca^{2+} spike frequency can optimize gene expression. Nature 392, 936–941.
Tzima E, Irani-Tehrani M, Kiosses WB, Dejana E, Schultz DA, Engelhardt B, Cao G, DeLisser H, Schwartz M (2005). A mechanosensory complex that mediates the endothelial cell response to fluid shear stress. Nature 437, 426–431.
Vittet D (2014). Lymphatic collecting vessel maturation and valve morphogenesis. Microvasc Res 96, 31–37.
Xu J, Mathur J, Vessières E, Hammack S, Nonomura K, Favre J, Grimaud L, Petrus M, Francisco A, Li J, *et al*. (2018). GPR68 senses flow and is essential for vascular physiology. Cell 9, 762–775.e16.
Yissachar N, Sharar Fischler T, Cohen AA, Reich-Zeliger S, Russ D, Shifrut E, Porat Z, Friedman N (2013). Dynamic response diversity of NFAT isoforms in individual living cells. Mol Cell 49, 322–330.
Yokota Y, Nakajima H, Wakayama Y, Muto A, Kawakami K, Fukuhara S, Mochizuki N (2015). Endothelial Ca^{2+} oscillations reflect VEGFR signaling-regulated angiogenic capacity *in vivo*. ELife 4, e08817.
Zhao M, Joy J, Zhou W, De S, Iii WHW, Becker KG, Ji H, Sen R (2018). Transcriptional outcomes and kinetic patterning of gene expression in response to NF-κB activation. PLoS Biol 16, e2006347.